Heterologous Expression of a Cryptic BGC from *Bilophila sp.* Provides Access to a Novel Family of Antibacterial Thiazoles

Maximilian Hohmann,[1] Denis Iliasov,[2] Martin Larralde,[3] Widya Johannes,[4] Klaus-Peter Janßen,[4] Georg Zeller,[3] Thorsten Mascher,[2] Tobias A. M. Gulder[1,5]

[1] Chair of Technical Biochemistry, Technical University of Dresden, Bergstraße 66, 01069 Dresden, Germany.

[2] Institute of Microbiology, Technical University of Dresden, Zellescher Weg 20b, 01217 Dresden, Germany.

[3] Center of Infectious Diseases, Leiden University Medical Center, Albinusdreef 2, 2333 ZA Leiden, Netherlands.

[4] Department of Surgery, School of Medicine, Klinikum rechts der Isar, Technical University of Munich, 81675 Munich, Germany.

[5] Helmholtz Institute for Pharmaceutical Research Saarland (HIPS), Department of Natural Product Biotechnology, Helmholtz Centre for Infection Research (HZI) and Department of Pharmacy at Saarland University, Campus E8.1, 66123 Saarbrücken, Germany.

Abstract

Human health is greatly influenced by the gut microbiota and microbiota imbalance can lead to the development of diseases. It is widely acknowledged that the interaction of bacteria within competitive ecosystems is influenced by their specialized metabolites, which act, e.g., as antibacterials or siderophores. However, our understanding of the occurrence and impact of such natural products in the human gut microbiome remains very limited. As arylthiazole siderophores are an emerging family of growth-promoting molecules in pathogenic bacteria, we analyzed a metagenomic dataset from the human microbiome and thereby identified the *bil*-BGC, which originates from an uncultured *Bilophila* strain. Through gene synthesis and BGC assembly, heterologous expression and mutasynthetic experiments, we discovered bilothiazoles A-F, new arylthiazole natural products. While established

activities of related molecules indicate their involvement in metal-binding and -uptake, which could promote the growth of pathogenic strains, we also found antibiotic activity for some bilothiazoles. This is supported by biosensor-experiments, where bilothiazoles C and E show P_{recA}-suppressing activity, while bilothiazole F induces P_{blaZ}, a biosensor characteristic for β-lactam antibiotics. These findings serve as a starting point for investigating the role of bilothiazoles in the pathogenicity of *Bilophila* species in the gut.

Introduction

The human gut hosts a large variety of microbial species, among them thousands of different bacterial species, which together form a complex ecosystem.(*1, 2*) A healthy gut microbiota is generally characterized by stable coexistence of symbiotic bacterial species and provides significant benefits for the host, such as colonization resistance against pathogenic bacteria, immunomodulation, and nutrient uptake.(*3, 4*) Alterations in bacterial composition, however, are linked to development of chronic diseases, including inflammatory bowel disease and colorectal cancer.

Microbial balance can be disrupted by a range of exogenous and endogenous factors, most notably antibiotic treatment, which can, e.g., lead to subsequent infections with *Clostridium difficile* or *Klebsiella oxytoca*.(*5, 6*) Host-produced antimicrobial peptides are recognized as an important factor to balance the intestinal microbiota. Such compounds can be produced by cells of the gastrointestinal tract and are a key component of the mammalian immune systems.(*7, 8*) In addition to such host-derived compounds, members of the gut microbiota possess their own, often strain-specific specialized metabolism, which can provide competitive advantages in this densely populated environment.(*9, 10*) Bacterial antibiotics are indeed a key component to understanding antagonistic microbe-microbe interactions in gut environments.(*11, 12*) These include a range of ribosomally synthesized and post-translationally modified peptides (RiPPs) with antibacterial activities.(*13, 14*) The importance to foster our understanding of the impact of such microbial natural products (NPs) is underlined by bioinformatic studies predicting the genetic capacity of the human gut microbiota to produce thousands of yet unknown NPs with unknown functions.(*15, 16*)

Apart from antibiotic activity, NPs can, e.g., act as siderophores, which can also influence microbe-microbe interactions in the gut. Well-characterized siderophores, such as yersiniabactin (ybt, **1**),

pyochelin (pch, **2**), or enterobactin (**3**) (Figure 1), facilitate bacterial iron uptake in competitive environments and play a significant role in the virulence of pathogenic bacteria such as *K. pneumoniae*, *Escherichia coli*, and *Pseudomonas aeruginosa*.(*17–19*) Compounds **1**-**3** are non-ribosomal peptides (NRPs), which is a family of NPs renowned for their broad range of bioactivities. NRPs are assembled from amino acid precursors by NRP synthethases (NRPSs), which are encoded by large genes organized in so-called biosynthetic gene clusters (BGCs) that can be readily identified by bioinformatic analysis of bacterial genomes using rule-based methods with tools such as antiSMASH.(*20*) Compounds **1** and **2** belong to the growing family of arylthiazole siderophores. Recently discovered members include the anthrochelins, for example antrochelin D (**4**)(*21*) from a human pathogen, and the myxobacterial sorangibactins.(*22*)

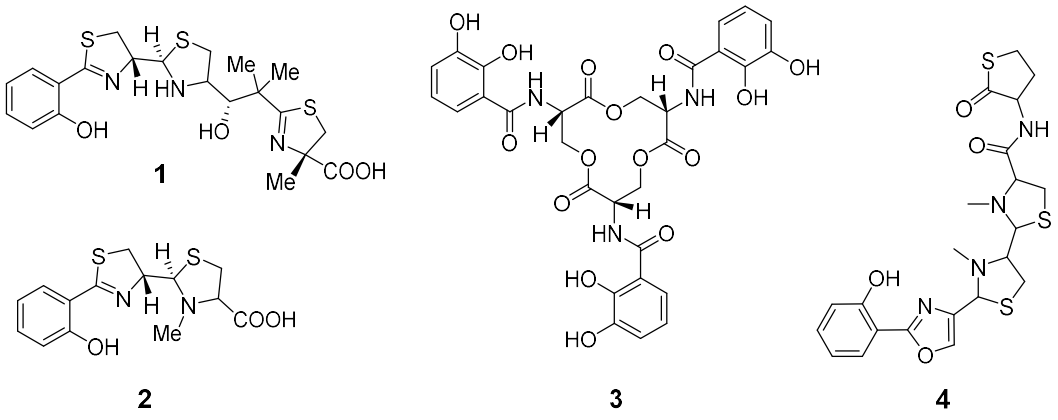

Figure 1. Structures of iron-chelating molecules yersiniabactin (**1**), pyochelin (**2**), enterobactin (**3**) and anthrochelin D/sorangibactin A (**4**). **1**, **2** and **4** share the arylthiazole/ -oxazole structural motif.

Virulence factors such as **1** also play important roles in gut environments. For example, it was shown that *E. coli* strains containing the *ybt* BGC promote inflammation-associated fibrosis in mice.(*23*) This suggests that siderophore systems in the gut microbiota are not only relevant for microbe-microbe- but also key to pathogenic microbe-host interactions. Our group is interested in accessing such yet undiscovered NPs from the gut microbiome with potential effects on microbiome composition and host health, but also with application potential in biomedicine. In this study, we bioinformatically analyzed a gut metagenomic dataset and identified a functionally uncharacterized BGC from uncultured *Bilophila sp.* putatively encoding an arylthiazole NP. The BGC was made available by gene synthesis and heterologously expressed in *E. coli*, leading to the isolation and characterization of new arylthiazole analogs, the bilothiazoles A–E (**5**–**10**), with antibiotic activity.

Results and Discussion

Bioinformatic Analysis

In previous studies, we identified the thiazol(in)e structural motif as a promising predictor of biologically active NPs in the gut.(*24*) Therefore, we explored two metagenomic datasets [Unified Human Gut Genome collection (UHGG)(*25*) and a gut-associated subset of proGenomes2(*26*)] for BGCs encoding NRPSs incorporating modules typically responsible for heterocyclization enzymology similar to *bac* BGC encoding the bacillamides. We then ordered the BGCs into Gene Cluster Families (GCFs) based on sequence similarity of their gene content (specifics see page 15, Figure 2a,b).(*27*) This led to the identification of the *bil* BGC, which was found to originate from an uncultured *Bilophila sp*. strain (Figure 2c). The related species *Bilophila wadsworthia* is a known pathobiont in the gut and was first isolated from infected appendices.(*28, 29*) More recently, it was shown to produce hydrogen sulfide in the gut, which is linked to the development of inflammatory bowel disease and colorectal cancer.(*30*) As there is only very limited knowledge of NPs from *Desulfovibrionia*, this makes the products of the *bil* BGC a promising starting point for NP discovery and for further evaluating the virulence and pathogenicity of this strain.

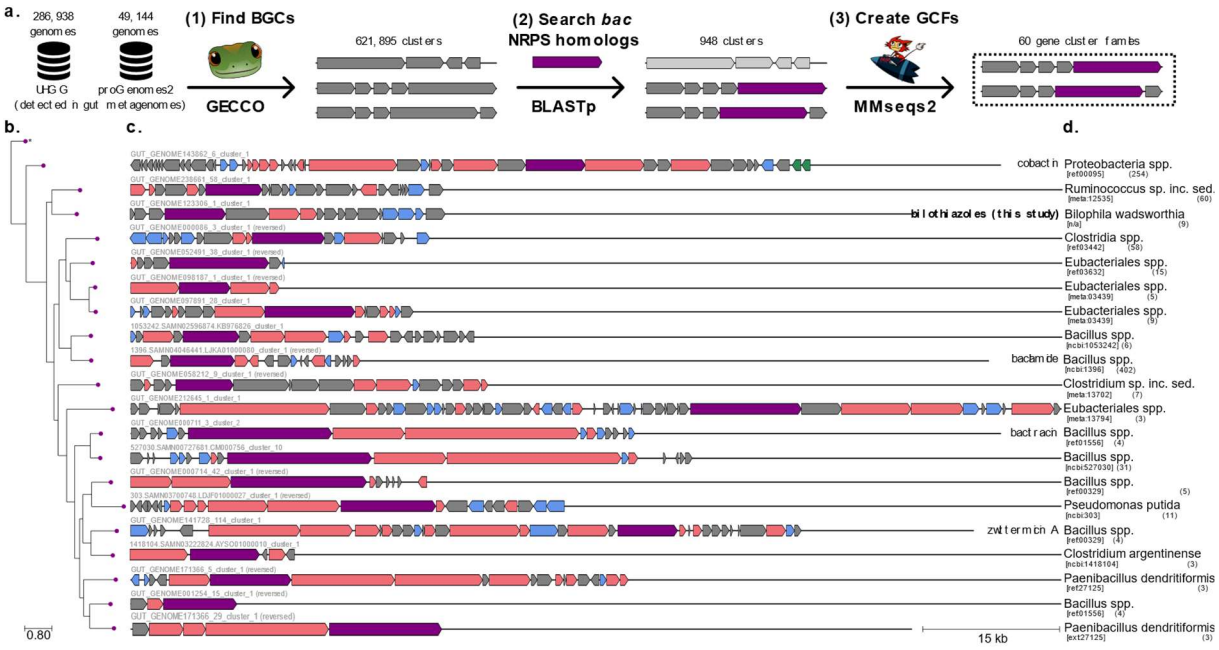

Figure 2. **a**. Bioinformatics workflow for identifying thiazole-producing BGCs. **b**. Phylogenetic tree of the NRPS proteins in the cluster representatives of the 20 most populated GCFs. The protein sequences of *bac* NRPS homologs were aligned using MUSCLE (v5.1 with default parameters).(*31*) The multiple sequence alignment was passed to FastTree2 (v2.1.11 with default parameters)(*32*) to build an approximately-maximum-likelihood

phylogenetic tree. The tree is displayed with the ETE Toolkit (v3.1.3).(*33*) **c**. The corresponding representative BGC for each GCF. The different cluster sequences were rendered using the dna-features-viewer package (v3.1.3).(*34*) Genes are colored according to the GECCO function prediction based on the Pfam domain content of each gene, either transporter (blue), biosynthetic (pink), regulatory (green) or unknown (grey); the *bac* NRPS homolog is shown in purple. Known BGCs that could be identified in literature have the produced compounds written on the right-hand side. **d**. The taxonomy and taxonomic identifiers of each cluster representative are shown in square brackets according to either the NCBI Taxonomy(*35*) for isolate genomes (ncbi), or to the mOTUs 3.1 taxonomy(*36*) for MAGs (ext, ref or meta). The number of BGCs in each GCF is shown in brackets.

The *bil* BGC is composed of fourteen genes *bilA–N*, including the three biosynthetic core genes *bilJ-L* encoding polyketide (PKS) and NRPS machinery with a total of 4 biosynthetic modules (Figure 3, Table S3). The AMP-ligase encoded by *bilI* shows a high degree of similarity to the 2,3-dihydroxybenzoate (DHB)-loading DhbE from *Bacillus subtilis* and the salicylate-loading PchD from the pyochelin (*pch*) pathway. The NRPS BilJ is similar to Irp2 from the yersiniabactin (*ybt*) BGC (33.0% identity) and to PchF (31.4% identity). The thioesterase encoded by *bilB* also shows similarities to these two pathways, but the *bil* BGC lacks the *N*-methyl transferase of the *pch* BGC and generally has a different architecture compared to *ybt*, therefore suggesting it to produce novel NP structures (see Figure S1). The gene *bilM* is predicted to encode another type II thioesterase and the AMP-ligase encoded by *bilE* is predicted to load 2,3-diaminopropionate (DAP), potentially offering another starting material. Core biosynthetic genes *bilJ* and *bilK* were not homologous to any characterized genes and the domain-structure of their encoded proteins, as assessed by Prism,(*37*) is depicted in Figure 3. In short, biosynthesis is expected to start with loading of either 2,3-DAP or 2,3-DHB onto the first T-Domain, followed by step-wise fusion with two cysteine moieties, which both should undergo heterocyclization catalyzed by the cyclization domains (Cy). This intermediate would then be further extended with a malonyl-CoA building block by PKS BilK and another, potentially *C*-methylated thiazol(in)e heterocycle by BilL.

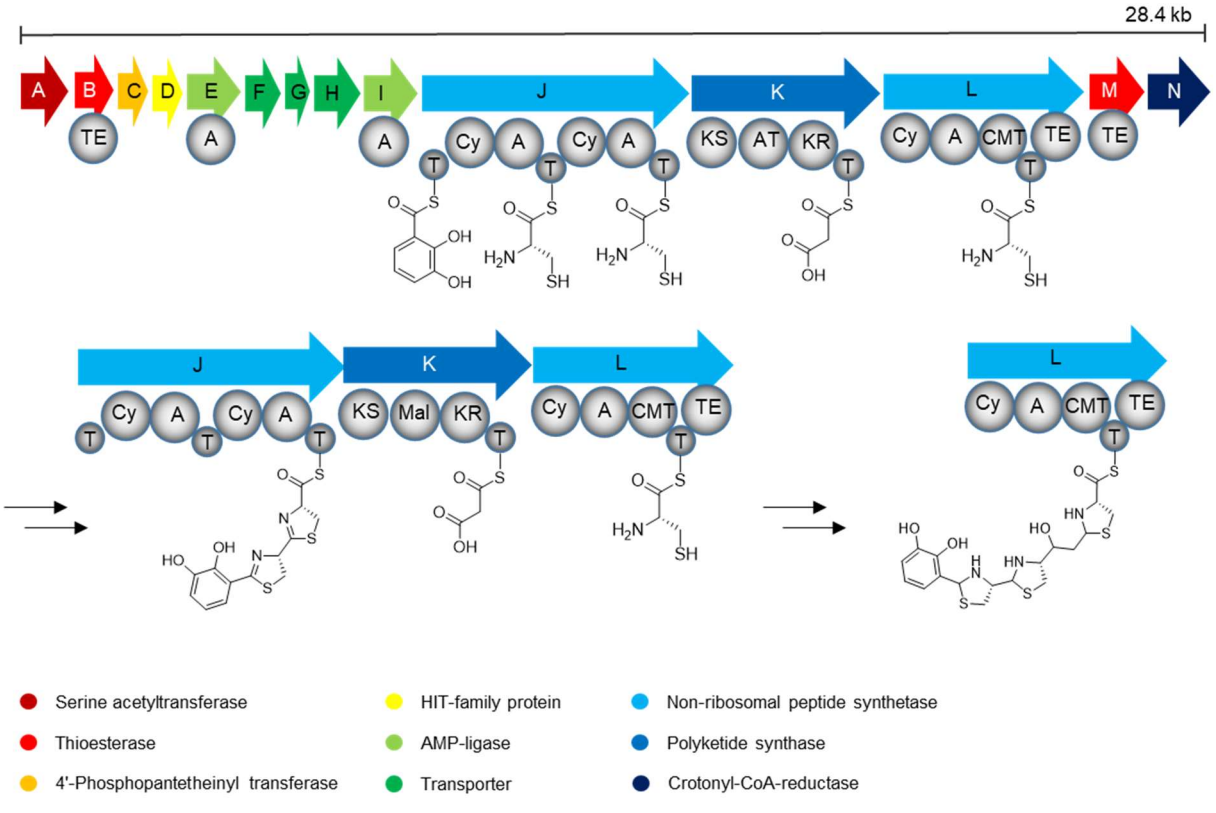

125

126 **Figure 3**. Architecture of the cryptic *bil* gene locus with predicted domain-structure of the NRPS/PKS-system and
127 potential intermediate products of PKS/NRPS-assembly. Instead of 2,3-DHB, also 2,3-DAP could be loaded onto
128 the first T-Domain. All other A-domains are predicted to activate cysteine. A: A domain, AT: acyltransferase domain,
129 Cy: cyclization domain, CMT: *C*-methyltransferase domain, KS: ketosynthase domain, KR: ketoreductase domain,
130 TE: thioesterase domain, T: thiolation domain.

131

132 **Cloning of the *bil* BGC**

133 The cloning of BGCs identified from metagenomic data is often not possible due to the lack of information
134 on the identity of the original BGC host strains and/or the lack of access to these strains or their gDNA.
135 A solution to this problem is the de-novo synthesis of the respective genetic sequence and its
136 subsequent introduction into a suitable expression vector for recombinant production. Construction of
137 the expression vector can readily be achieved using Direct Pathway Cloning.(*24, 38–42*) Following this
138 approach, we selected twelve of the 14 genes of the *bil* BGC to be included in the final expression
139 construct. Gene *bilC*, encoding for a putative phosphopantetheinyl transferase (PPTase), was omitted
140 as the foreseen heterologous expression strain *E. coli* BAP1 harbors the promiscuous PPTase Sfp.(*43*)
141 Gene *bilD* encoding a HIT-family protein was not thought to have a biosynthetic function and was thus
142 likewise not included. Due to general size limitations in commercial gene synthesis, all other target

genes were redistributed over four synthetic gene fragments, including the PKS-encoding genes *bilKL* (fragment I, dark blue, size: 9956 bp), the NRPS-encoding gene *bilJ* (fragment II, light-blue, size: 6690 bp), genes *bilABEI* (fragment III, green, size: 4959 bp), and genes *bilMNFGH* (fragment IV, yellow, size: 4966 bp) (Figure 4a). All genes were codon-optimized for expression in *E. coli*. Genes *bilKL* were directly integrated into the vector backbone pET28b-ptetO::*gfp* to yield vector construct I. Starting from I, the cluster was reassembled into expression vectors V, VI, VII and VIII in a stepwise manner, as depicted in Figure 4b.

Assembly of vector construct V involved linearization of I by restriction digest with EcoRI and ligation with the excised gene *bilJ* from fragment II, digested with the same restriction enzyme. Expression vectors VI and VII were assembled from V utilizing SLIC.(*44*) Briefly, V was linearized with restriction digest and the insert fragment was amplified by PCR from its synthetic vector, attaching 23-25 bp homology arms, followed by SLIC-assembly to yield the circular expression plasmid. The complete plasmid VIII was assembled from VI in an analogous fashion. Pictures of the SDS-gel analyses for cloning, colony screening, and restriction digests are provided in the supplementary information (Figures S2–S5). Plasmids V and VI were also validated by sequencing (Figures S6, S7). This method of stepwise construct assembly furthermore enabled comparative metabolomics between the differentially equipped expression constructs.

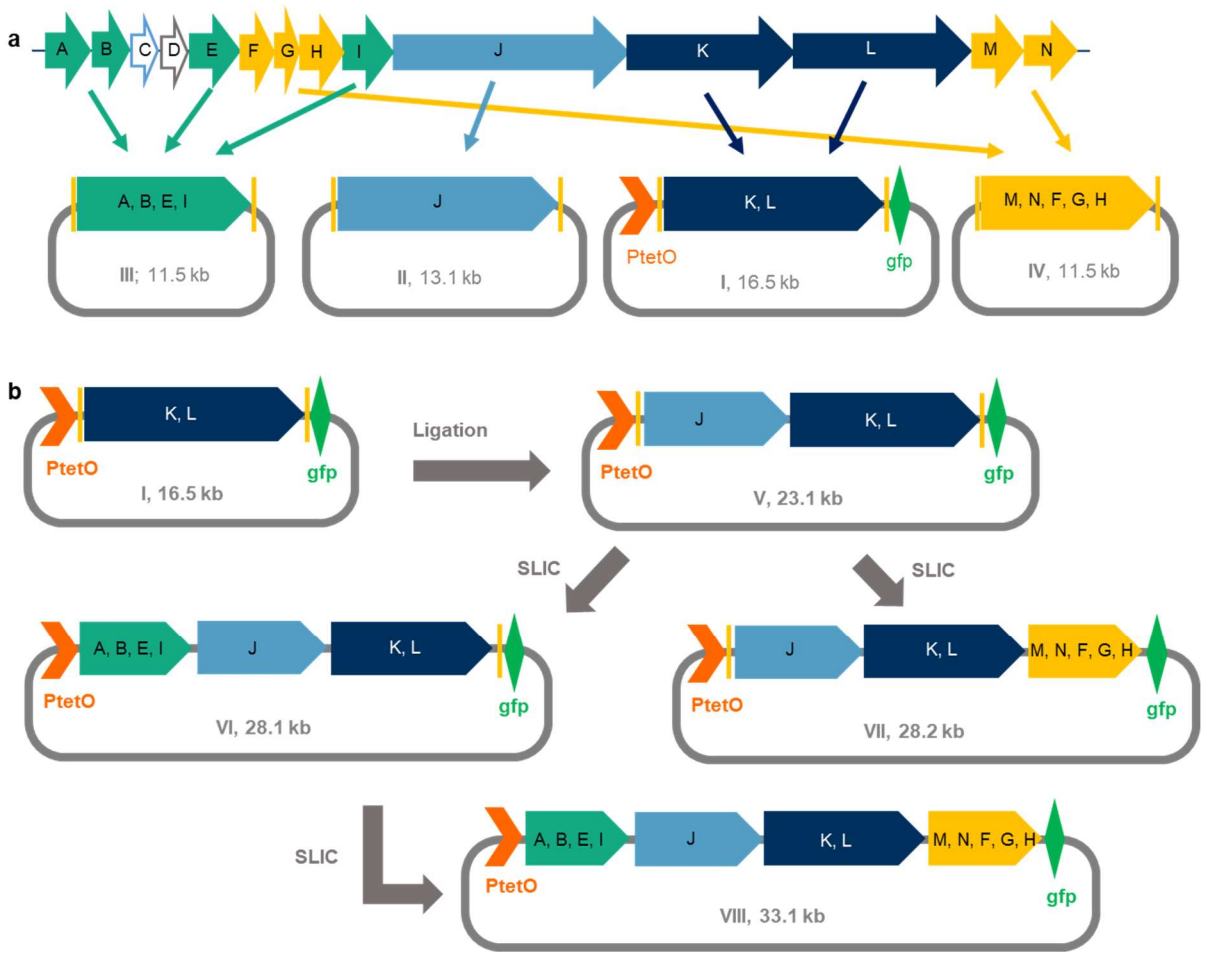

Figure 4. The cloning strategy for the *bil* BGC. **a**. Reogranization of the biosynthetic genes into four synthetic plasmids (I, dark blue, *bilKL*; II, light blue, *bilJ*; III, green, *bilABEI*; IV, yellow, *bilMNFGH*). **b**. Schematic representation of cloning strategy for stepwise assembly of the expression vectors V–VIII by Ligation and SLIC.

Heterologous Expression and NP isolation

The expression vectors V–VIII were amplified by transformation and cultivating *E. coli* DH5α with subsequent plasmid isolation, followed by transformation into the recombinant host of choice, *E. coli* BAP1. Heterologous expression was tested in TB, LB, and M9-media (100 mL each) for durations of 64 and 122 h after induction with tetracycline. Cells were separated from spent media by centrifugation and both samples were extracted with ethyl acetate. Initial heterologous expression experiments using vectors VI and VIII in M9 medium led to the production of a new compound eluting at 14 min during HPLC analysis, which was not present in control expressions using the empty vector pET28b-ptetO-*gfpV2* (Figure 5a). As the production titer of this molecule using construct VI was slightly higher, all

further expressions were carried out with this plasmid. In expressions with the constructs not containing insert III (V and VII), the compound eluting at 14 min was not observed.

After initial isolation from small-scale cultures (100 mL M9), it was found that the HPLC-UV signal detected at 14 min corresponded to a mixture of two co-eluting compounds with molecular masses at *m/z* 323.0153 $[M+H]^+$ (**5**) and *m/z* 341.0260 (**6**). However, the production yield at this cultivation scale turned out to be too low for compound characterization by NMR. The *m/z*-values corresponded to calculated chemical formulae of $C_{13}H_{10}N_2O_4S_2$ ($[M+H]^+$ = 323.0155) for **5** and $C_{13}H_{12}N_2O_5S_2$ ($[M+H]^+$ = 341.0260) for **6**. Given the structural predictions for the *bil* assembly line (Figure 3), this suggested a potential offloading of the NRPS product **5** by thiolysis from the final T domain of NPRS BilJ, with subsequent partial hydrolytic opening of the thiazoline ring to give **6** (Figure 5c). For both molecules, the incorporation of a 2,3-dihydroxybenzoic acid (DHBA) starter unit was thus assumed. To increase production of **5** and **6**, expression cultures were supplemented with 125 μM 2,3-DHBA, which indeed greatly enhanced the production titer (from approx. 0.1 mg/L to 3.8 mg/L), thereby enabling compound isolation and NMR structure analysis in DMSO-d_6.

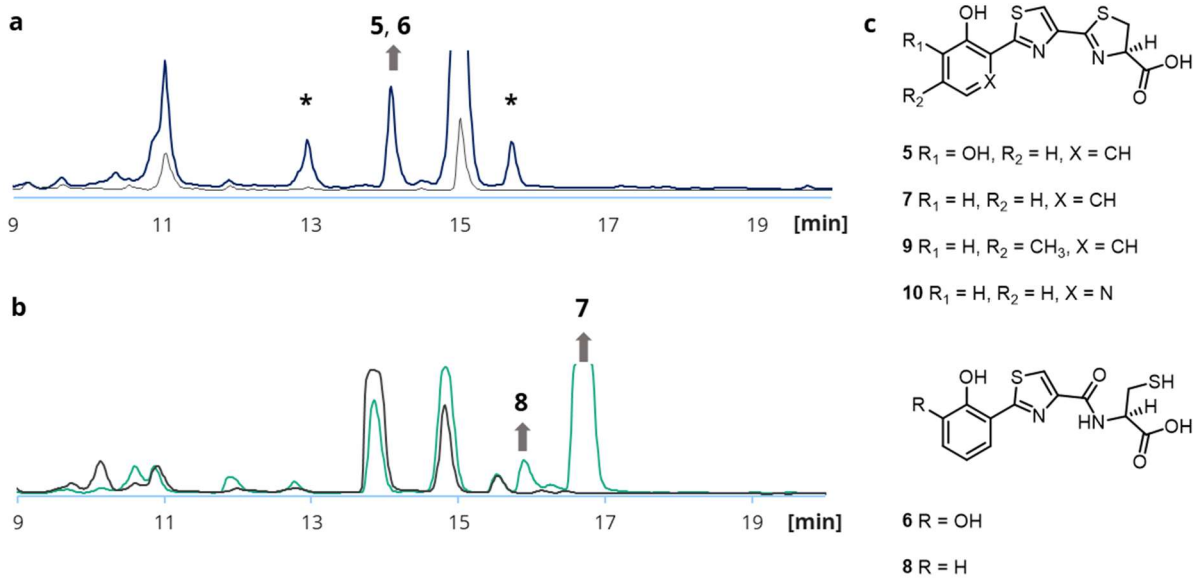

Figure 5. **a**. Identification of **5** and **6** in extracts of culture supernatants of cultures of *E. coli* BAP1 after 50 h with construct **VI** in M9 medium (blue), compared to negative control (grey). (*) These compound had molecular masses that were also present in the control expression, albeit at significantly lower abundance. **b**. Identification of **7** and **8** in extracts of salicylic-acid-supplemented cultures (blue-green), compared to negative control (grey). **c**. Structures of bilothiazoles A and B (**5** and **6**), C (**7**), D (**8**), E (**9**) and F (**10**).

The proposed chemical formulae for the identified masses indicated 10 and 9 double bond equivalents for **5** and **6**, respectively. The ^{1}H-NMR spectrum conferred the presence of several aromatic hydrogens, six of which could be designated to two coexisting DHB-moieties by ^{1}H-COSY. The signal sets for **5** and **6** were very similar, except for the chemical shifts of the thiazoline/cysteine, which are located at $\delta(^{1}H)$ = 5.31 and 3.62 ppm for **5** and 4.65 and 3.05 ppm for **6** (see Figure S22). The cysteine-moiety of **6** is marked by the presence of an adjacent nitrogen-bound hydrogen, as determined by 2D-NMR (^{1}H-COSY, ^{1}H, ^{13}C-HSQC). Further ^{1}H, ^{13}C-HMBC-analysis confirmed the existence of a thiazole in each molecule, connecting the aforementioned structural elements (Figure 6). In conclusion, these analyses confirmed the initially proposed structures of the isolated NPs, which can thus be classified as shunt products of the *bil*-biosynthetic pathway, resulting from premature hydrolytic offloading from BilJ. The originally anticipated end product of the *bil* BGC remained absent in our heterologous expression experiments. Nonetheless the discovery of **5** and **6** is of interest, as to our knowledge, these structures have not been reported before.

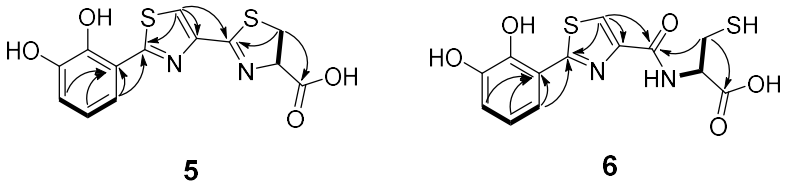

5 **6**

Figure 6. Chemical structures of bilothiazoles A (**5**) and B (**6**) with key COSY (bold) and HMBC (arrows) correlations.

Mutasynthetic studies for NP diversification

Given the greatly enhanced production titers when feeding the 2,3-DHBA NRPS starter unit, a mutasynthetic approach was tested to evaluate opportunities for compound structural diversification. A total of 18 additional benzoic acid derivatives was thus screened as culture supplements. Ten of these did not result in any product formation (see Table S4 for details). For benzoic acid, 3-hydroxy benzoic acid, 4-amino salicylic acid, vanillic acid and *ortho*-vanilic acid, small amounts of the expected NP analogs were detectable by HR LC-MS (Figures S8–12), unfortunately at yields too low for compound isolation. Supplementation with salicylic acid (products **7** and **8**, 33.3 mg/L and 3.9 mg/L, Figure 5b), 4-methyl salicylic acid (**9**, 9.8 mg/L), or 3-hydroxy picolinic acid (**10**, 1.9 mg/L) led to the formation of sufficient quantities of products for isolation and structural characterization (Figure 5c). Bilothiazole C (**7**) was previously reported in literature as “HPTT-COOH” and its ^{1}H and ^{13}C-NMR spectra were in

agreement to the reported data.(*45*) Bilothiazole D (**8**) was easily distinguishable from **7** by the presence of a nitrogen-bound hydrogen and the different chemical shifts of the cysteine not involved in heterocyclization ($\delta(^1H)$ = 4.86 and 3.15 ppm, spectrum in Figure S33). HPTT-COOH (**7**) and HPT-Cys (**8**) were previously identified as intermediates in pyochelin biosynthesis but no bioactivities had been determined.(*46, 47*) Compound **7** has also been found to be a byproduct of yersiniabactin-biosynthesis, detected in urinary tract infections, and possibly playing a protective role against *Pseudomonas*.(*48*)

Bilothiazole E (**9**) featured the expected methyl-group attached to the aromatic system ($\delta(^1H)$ = 2.29 ppm, $\delta(^{13}C)$ = 21.1 ppm, Figure S39) and the NMR spectroscopic data was otherwise in line with those of **7**. For **10**, the aromatic system matched the expected chemical shifts for 3-hydroxy-picolinic acid ($\delta(^1H)$ = 8.25, 7.56, 7.49), with again comparable NMR data with respect to **7** (Figure S45). Overall, this work thus proved some degree of starter unit promiscuity by the loading A domain of the *bil* BGC, facilitating incorporation of four out of a total of 19 tested starter units.

The BGC encodes two alternative free-standing A-domains, BilE and BilI, which could perform *in-trans* starter-unit selection and activation for NRPS-assembly (Figure 3). Bioinformatic sequence analysis predicts BilE is to load 2,3-diaminopropionate, while BilI is predicted to activate salicylate and, to a lesser extent, 2,3-DHB. Evaluation of the heterologous expression experiments leads to the conclusion that BilE is not involved in precursor recruitment or inactive in the recombinant production system (no products with 2,3-diaminopropionate starter unit), while BilI is indeed capable of accepting salicylic acid, 2,3-DHB, and the above mentioned structural analogs. While molecule **5** incorporating 2,3-DHB was the main product of unsupplemented expressions of the *bil* BGC, we also found evidence for formation of **7** incorporating salicylic acid in LC-MS data of raw extracts of unsupplemented expression cultures, thus suggesting both molecules to be NPs. The lower abundance of **7** (about 1% of **5**, see Figure S13) might rather be a result of limited starter unit availability in *E. coli*, as the alternative building block 2,3-DHB is also produced in the biosynthesis of the siderophore enterobactin.(*49, 50*) However, salicylate seems to actually be the preferred substrate of the BGC, since it showed the highest production titer of all tested substrates within our mutasynthetic experiments (Table S4).

It is interesting to note that the formation of the open-chain derivatives **6** and **8** stem from hydrolysis of the thiazoline ring in **5** and **7** after their biosynthetic assembly. This was suspected to be catalyzed by acidic conditions, e. g., during extraction from the culture broth or HPLC/MPLC-purification. In raw extracts of expressions supplemented with 2,3-DHBA, the ratio of **5** to **6** was roughly 13:1, as assessed

by MS (Figure S14). After purification, the ratio changed to 4:5, as determined by ^{1}H-NMR (based on the characteristic peaks of the terminal cysteine for **6** at δ = 4.65 and 3.05 ppm, Figure S22). This occurred despite choosing a non-TFA-supplemented mobile phase during chromatographic purification, indicating a lability of the molecule already under neutral conditions. In contrast to the mixture of **5** and **6**, compound **7** had a longer retention time compared to its open-chain derivative **8** and therefore their separation was readily achieved by prep-HPLC. Interestingly, both, compounds **9** and **10**, seemed far less prone to ring-opening and only traces of their ring-opened forms were detected.

Bioactivity

As the thiazole structural moiety had previously been linked to DNA-binding activity and thiazole-containing molecules in the gut are known as genotoxins(*51, 52*) and cytotoxins,(*24*) we initially tested the activity of NPs **7** and **8** against HCT116 cells. These substances were selected due to their higher availability and easier purification, compared to the others, and to determine whether the open or closed state of the thiazoline-ring had an effect on activity. While it was confirmed that **7** is readily taken up into the cytosol (Figure S15), inhibitory activity was only observed at concentrations >250 µM in clonogenic survival assays (Figure S16). In contrast, almost no uptake of **8** into the cells was observed, which consequently showed no cytotoxic activity. For more accurate quantification, the activities of bilothiazoles C–E (**7**–**9**) were analyzed in SRB-assays, which again turned out to be weak (Figure S17).

Next, we turned to the evaluation of antibacterial activity. In overlay-assays, inhibitory activity against a panel of gram-positive and -negative bacteria was tested. This indicated weak inhibition of *B. subtilis* and *Staphylococcus aureus* upon treatment with **7** and, to a lesser extent, **8** (Figure S18). Given the presence of the *bil* BGC in the human gut metagenome, this encouraged further tests of all molecules produced by the BGC, including mutasynthetic analogs, against these bacterial pathogens. While **5**, **6** and **8** were generally less effective against bacterial strains, mutasynthetic derivatives **9** and **10** showed the most potent, yet still rather weak effects at an inhibition of up to 83.8 µg/mL for **9** against *B. subtilis* (Figure S19). Compound **9** was the only bilothiazole inhibiting the growth of *S. aureus*. When tested against *Penicillium chrysogenum*, none of the NPs displayed antifungal properties (see Table S5, Figures 7a and b).

In a follow-up experiment, we aimed to get further insights into the potential molecular targets of the antibacterial bilothiazoles. Therefore, we employed *B. subtilis* whole-cell biosensor strains, containing a promoter (P_{recA}, P_{blaZ}, P_{liaI}, P_{bceA}, P_{psdA}, P_{yrzI}, P_{helD}, Py_{fiLMN}) fused to a luciferase cassette. The induction

and activity of the used promoters results in bioluminescense that can be quantified by plate-reader assays. For the bilothiazoles, we identified two separate potential functions: bilothiazoles C (**7**) and E (**9**) were found to strongly repress the P_{recA}-promoter (>10-fold) in *B. subtilis* upon treatment (Figure 7c, Figure S20), which indicates their involvement in the repression of DNA-repair. Recombinases from the RecA-family are found in virtually all bacteria and are regulated within the SOS-stress-response.(*53, 54*) However, the mechanism underlying the RecA-repression of **7** and **9** remains unknown.

Interestingly, bilothiazole F (**10**) was instead found to induce the P_{blaZ}-biosensor, which is characteristic for β-lactam antibiotics (Figure 7d, Figure S21). BlaZ is a β-lactamase, conferring resistance to these antibiotics by hydrolysis of the β-lactam ring.(*55, 56*) While **10** does not possess this structural moiety, these results might indicate the compound to also inhibit transpeptidases and therefore induce β-lactamase activity.

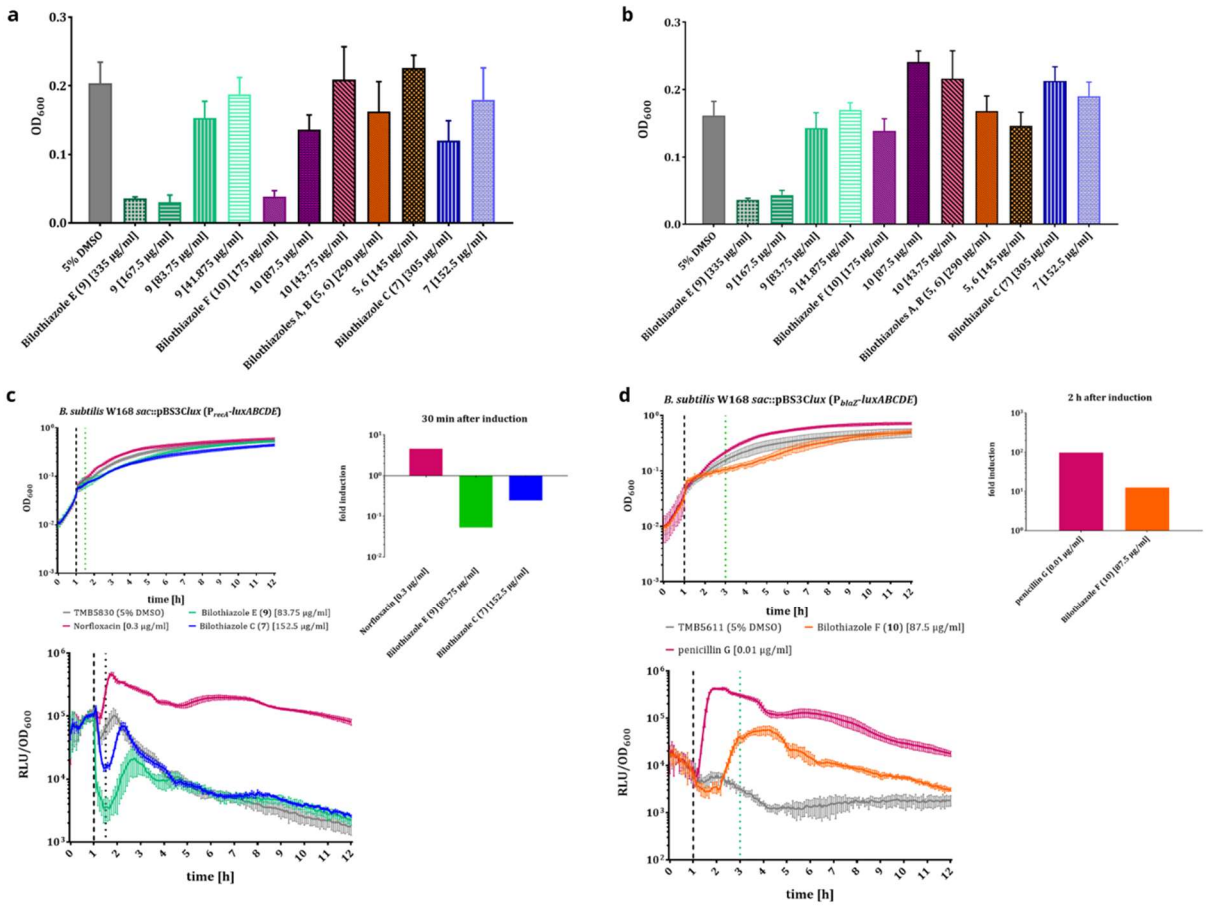

Figure 7. Antibiotic activity of the bilothiazoles: **A**. OD600 measurements 3 h after treatment: **9** and **10** show the strongest activity against *B. subtilis* W168. **B**. OD600 measurements 3 h after induction: only **9** is active against *S. aureus*. **C**. Repression of the P_{recA}-promoter by **7** and **9** compared to positive control (norfloxacin). **D**. Induction of P_{blaZ}-promoter by **10**, compared to positive (penicillin G) and negative control.

Conclusion

In conclusion, we report the discovery of the *bil*-BGC from a metagenomic dataset, its assembly from synthetic DNA into several different expression vectors, and its heterologous expression in *E. coli* leading to the discovery of the new NPs bilothiazoles A (**5**) and B (**6**). Furthermore, mutasynthetic experiments revealed some degree of substrate promiscuity concerning the NRPS starter unit, which allowed for the production of bilothiazole derivatives **7**–**10**. Among those, **7** and **8** were previously known as intermediate products of pyochelin biosynthesis, and **7** is known to possess Fe(III)-binding activity.(*48*) Since the biosynthesis of the bilothiazoles can be entirely explained without *bilK* and *bilL*, the observed compounds are shunt products of the *bil* BGC. However, in our heterologous expressions under varied expression conditions, we did not find evidence for a larger final product of the *bil*-BGC. This indicates that *bilKL* might be inactive under our culture conditions or that the final product is unstable outside the cells. This phenomenon is known from other BGCs putatively encoding thiazol(in)e-containing products, such as the enigmatic coelibactin from *Streptomyces coelicolor* A3(2).(*57*)

Furthermore, in-depth biological activity testing revealed that the bilothiazoles show weak antibacterial activity. While **7** and **9** were found to suppress the P_{recA}-promoter, indicating inhibition of DNA-repair, **10** surprisingly induced P_{blaZ}, which might indicate inhibitory effects on transpeptidases. These findings shed light on the metabolism of *Bilophila* species, bacterial strains that possibly have detrimental effects on gut health. Members of the *Bilophila* genus have been linked to appendiceal infections and hydrogen sulfide production in the intestine, which has effects on disease pathology. Further studies on the bilothiazoles are currently underway in our group to better understand their potential role in human intestinal health.

Materials and Methods

Strains, Plasmids, Cell lines, Enzymes

Bacterial strains and plasmids used in this study are listed in Table S1. *E. coli* strains were cultivated at 37 °C in LB medium supplemented with a suitable selection antibiotic while shaking at 180 rpm, or on LB-Agar supplemented with selection antibiotic at 37 °C unless otherwise specified. DNA was kept in MilliQ water for short-term storage. For long-term storage, plasmids were transformed into *E. coli* DH5α and cryostocks (75% LB-medium, 25% glycerol) were stored at −80 °C. *B. subtilis* and *S. aureus* were

routinely grown in Lysogeny broth (LB-Medium (Luria/Miller), Carl Roth GmbH & Co., KG, Karlsruhe, Germany) at 37 °C with agitation. 1.5% (w/v) agar (Agar-Agar Kobe I, Carl Roth GmbH & Co., KG, Karlsruhe, Germany) was added to prepare the corresponding solid media. Due to their BSL-2 status, all experiments involving BSL-2-microorganisms were conducted in a BSL-2 laboratory (Institute for Microbiology, TU Dresden, Dresden, Germany).

All restriction enzymes for this study were purchased from NEB. Culture supplements were generally dissolved to 1 M or 0.5 M stock solutions in DMSO.

Bioinformatics

We applied GECCO (v0.9.2)(*58*) to a set of 49,144 isolate genomes of bacterial species and 286,938 metagenome-assembled genomes (MAGs) originating from the human gut.(*25, 26*) GECCO predicted 621,895 candidate biosynthetic gene clusters (BGCs). We screened the GECCO predictions to find BGCs containing homologs to the *bac* NRPS,(*24*) using *blastp* (NCBI BLAST+ v2.5.0 with default parameters),(*59*) yielding 948 clusters with at least one hit. We then clustered the selected clusters into Gene Cluster Families (GCFs) using MMseqs2 linclust pipeline (MMseqs2 v13.45111 with --cov-mode 1 --cluster-mode 1 -c 0.7 –min-seq-id 0.5),(*60*) yielding 60 GCFs including 29 singletons. Further analysis of BGCs was performed with AntiSMASH (Version 6) (*20*) and PRISM (Version 3)(*37*). All sequences and plasmids were analysed, edited and saved in the Geneious software package (Version 8.1.9).(*61*) Gene cluster comparison was performed with Clinker (https://cagecat.bioinformatics.nl/)(*62*) using standard input paramenters.

Cloning

Constructs for this study were prepared either by ligation cloning (pET28b-ptetO::7246p1+2_*gfp*) or SLIC (all other constructs). For the ligation step, linearized fragments of insert and backbone were prepared by preparative restriction digest with EcoRI and purified by gel extraction. The linearized backbone fragment was dephosphorylated with Antarctic phosphatase (NEB) prior to purification to prevent re-ligation. The ligation reaction was performed with T4 DNA ligase (NEB) using 0.02 pmol of linearized backbone and 0.06 pmol insert. For SLIC-cloning, linear fragments of the inserts were generated by PCR using primers listed in Table S2 and plasmids listed in Table S1. In general, homology arms of 20–25 base pairs were used and placed on the insert fragment by PCR with Q5-Polymerase (NEB) in 50 µL batches consisting of: 1 x Q5 reaction buffer, 200 µM dexynucleotide triphosphates, 500 nM of forward and reverse primer, 10 ng plasmid-template and 0.01 U/µL Q5 High-Fidelity DNA

polymerase (NEB). Thermal cycling was performed in a T100 Thermal Cycler (Bio-Rad) as follows: 1.) Initial denaturation, 98 °C for 30 sec.; 2.) Denaturation, 98 °C for 10 sec.; 3.) Primer annealing for 20 sec.; 4.) Extension, 72 °C for 40 s/kb; 5.) Final extension, 72 °C for 5 min. Steps 2.) to 4.) were repeated for 30 cycles in total. The annealing temperatures for specific primer pairs were estimated with the NEB Tm Calculator tool (https://tmcalculator.neb.com/). Vector backbones were linearized by restriction digest as described previously. SLIC-cloning was performed as described previously.(*39*)

Transformants were selected on LB-agar plates with kanamycin (kan) as selection antibiotic and initially screened by colony-PCR using Onetaq polymerase (NEB) for correctly assembled constructs. Clones were picked, resuspended in 12 µL of LB-medium supplemented with kan, and examined in a 25 µL PCR reaction composed as following: 1 x Onetaq Buffer, 200 µM deoxynucleotide triphosphates, 200 nM of forward and reverse primer, 2 µL cell suspension (DNA template) and *Onetaq* DNA polymerase (NEB). Thermocycling conditions were set as described above, with the exception of 94 °C denaturation and 68 °C extension temperatures. Positive clones were confirmed by restriction digest, terminal-end Sanger sequencing by Azenta and additionally full plasmid sequencing by SNPsaurus.

Analytical and preparative HPLC

Analytical high-performance liquid chromatography (HPLC) was performed on an Azura HPLC device manufactured by Knauer, consisting of the following components: AS 6.1L sampler, P 6.1L pump, DAD 2.1L detector. Components were separated on a Phenomenex Luna 3u C-18 column (150 × 4.6 mm) at a flowrate of 1 mL/min with the eluents water (A) and acetonitrile (B), both supplemented with 0.05% trifluoracetic acid. The elution method consisted of equilibration at 5% B for 2 min, followed by a gradient of 5–100% B over 28 min. Column washing was performed at 100% B for 5 min and the column was re-equilibrated at 5% B for 2 min before the next measurement.

Preparative HPLC was performed on a Jasco HPLC system consisting of an UV-1575 Intelligent UV/Vis detector, two PU-2068 Intelligent preparation pumps, a Mika 1000 dynamic mixing chamber (1,000 µl; Portmann Instruments AG Biel-Benken) and a LC-NetII/ADC anda Rheodyne injection valve. The system was controlled by Galaxie software. Chromatographic separation was performed on a Eurospher II 100-5 C18 A (250 × 16 mm) column with precolumn (30 × 16 mm) provided by Knauer at a flow-rate of 10 ml/min and the eluents were water (A) and acetonitrile (B). The gradient was adjusted depending on the polarity of the compounds. Collected product fractions were combined, the organic solvent was evaporated under reduced pressure at 40 °C and water was removed by lyophilization.

MPLC Purification

Medium-pressure liquid chromatography (MPLC) was conducted on a Büchi Pure C-800 Flash MPLC system with a Reveleris 40 µm C18 cartridge (12 g) with the eluents water (A) and acetonitrile (B). Purification was generally achieved with a 20–40% B gradient over 20 min, followed by a 40–80% B gradient over 5 min. Collected product fractions were combined, the organic solvent was evaporated under reduced pressure at 40 °C and water was removed by lyophilization.

HR LC-MS measurement

For liquid chromatography (LC) coupled to high resolution mass spectrometry (HR-MS), a Bruker Elute UHPLC-system with an Intensity Solo 2 C18-column (100 × 2.1 mm) coupled to a Bruker Impact II ultra-high resolution Q TOF mass spectrometer with electron-spray ionization (ESI) were used. For LC, water (A) and acetonitrile (B) were used as eluents, both supplemented with 0.1% formic acid, at a flow-rate of 0.3 mL/min. The elution method consisted of equilibration at 5% B for 2 min, a gradient of 5–95% B over 23 min, washing at 95% B for 3 min and re-equilibration at 5% B for 2 min.

General procedure for heterologous expression and extraction of organic molecules

Culture conditions for heterologous expression experiments were based on those described previously for the pET28b-ptetO-*gfp* vector system.(*40, 63*) The desired expression plasmids and pET28b-ptetO-*gfp* (empty) as a negative control were individually chemically transformed into *E. coli* BAP1 and selected on an LB-agar plate containing kanamycin. Precultures were inoculated from a single colony, grown in LB-medium o/n and used to inoculate expression cultures with 1% (vol/vol) in TB, LB or M9-medium. Expression cultures were incubated while shaking at 180 r.p.m. at 37 °C until an OD_{600} of 0.8 for TB and LB cultures or 0.4 for M9 cultures was reached and subsequently cooled to 4 °C for 60 min. Expression was induced by adding 0.5 µg/mL tetracycline and varying amounts of culture supplement when applicable. The cultures were incubated at 20 °C while shaking at 180 r.p.m in darkness. Test expressions were performed in 100 mL scale in 250 mL Erlenmeyer flasks for 3 and 5 days, respectively; upscaled expressions in 1 L growth medium in 2 L Erlenmeyer flasks.

After incubation, cultures were centrifuged (6000 g for 15 min) to separate *E. coli* biomass from growth medium. The culture supernatants were adjusted to a pH of 3–4 by addition of conc. HCl and extracted with ethyl acetate (2 × 80 mL per 100 mL of growth medium). The combined extracts were washed with saturated brine, dried over $MgSO_4$, and filtered. The solvent was removed under reduced pressure at

40 °C. Dried extracts were redissolved in HPLC-grade methanol and filtered through a syringe driven 0.2 µm PTFE membrane filter (Fisherbrand, USA) prior to HPLC analysis.

Heterologous expression and isolation of bilothiazoles A and B (5 and **6)**

A preculture was inoculated from a cryostock of *E. coli* BAP1 containing the plasmid pET28b-ptetO::7246p1+2+T1_gfp (VI). The expression was supplemented with 125 µM 2,3-DHBA and carried out in 8 L of M9-medium for 3 days. After extraction, the crude extract was purified on a MPLC system with a gradient of 15–40% B over 20 min, where the products eluted between 8 and 13 min. A mixture of **5** and **6** was isolated as yellow-brown oil (30.6 mg; 3.8 mg/L)

Heterologous expression and isolation of bilothiazoles C and D (7 and **8)**

A preculture was inoculated from a cryostock of *E. coli* BAP1 containing the plasmid VI. The expression was supplemented with 250 µM salicylic acid and carried out in 4 L of M9-medium for 5 days. After extraction and evaporation of the organic phase, **7** precipitated as beige crystalline substance and was washed with cold methanol to remove other organic components. 133 mg of **7** were collected (33.3 mg/L). The methanol fraction was purified on an MPLC system with a 20–40% B gradient over 20 min, where **7** and **8** eluted as a mixed fraction between 15 and 18 min. Compound **8** was subsequently purified by preparative HPLC using a gradient from 30–50% B over 20 min where it eluted at 17 min. Compound **8** was isolated as white crystals (15.5 mg; 3.9 mg/L).

Heterologous expression and isolation of Bilothiazole E (9)

A preculture was inoculated from a cryostock of *E. coli* BAP1 containing the plasmid VI. The expression was supplemented with 250 µM 4-methylsalicylic acid and carried out in 8 L of M9-medium for 5 days. The crude extract was purified on a MPLC system as described before with an adjusted gradient of 20-45% B over 25 min, where the product eluted between 16 and 21 min. Compound **9** was isolated as white crystals (78,2 mg; 9.8 mg/L).

Heterologous expression and isolation of Bilothiazole F (10)

A preculture was inoculated from a cryostock of *E. coli* BAP1 containing the plasmid **VI**. The expression was carried out in 4 L M9-medium and supplemented with 125 µM 3-hydroxy picolinic acid. The crude extract was purified on a MPLC system as described before, where a crude product eluted between 10 and 14 min. Final purification ensued by preparative HPLC with a gradient of 35–50% B over 15 min, where the product eluted at 12 min. Compound **10** was isolated as yellow solid (7.5 mg; 1.9 mg/L).

Specific rotation

Specific rotations were measured with a Krüss P3000 polarimeter at 20 °C in methanol. Concentrations *c* are given in mg/mL.

NMR-measurement

^{1}H and ^{13}C Nuclear Magnetic Resonance spectra (NMR) were recorded on Bruker AVANCE 300 and AVANCE 600 spectrometers at room temperature. The chemical shifts are given in δ-values (ppm) downfield from TMS and are referenced on the residual peak of the deuterated solvents (DMSO-d_6: δ_H = 2.50 ppm, δ_C = 39.5 ppm, Methanol-d_4: δ_H = 3.31 ppm, δ_C = 49.1 ppm). The coupling constants *J* are given in Hertz [Hz].

Spot-on-lawn Assay

Screening for antimicrobial activity of purified bilothiazoles was performed by plate-spreading soft agar inoculated with a bacterial or fungal strain (Gram-positive *B. subtilis* W168, *B. subtilis* subsp. *spizizenii* ATCC 6633, *S. aureus* ATCC 25923 and *Enterococcus faecalis* ATCC 29212; Gram-negative *E. coli* K12, *P. aeruginosa* ATCC 27853 and *Enterobacter cloacae* ATCC 23355; *P. chrysogenum*). Due to their BSL-2 status, all experiments involving these microorganisms were conducted in a BSL-2 laboratory (Institute for Microbiology, TU Dresden, Dresden, Germany). The overnight cultures of the bacterial strains were inoculated in LB medium. Next, day cultures of the antagonist strains were inoculated 1:250 in fresh LB w/o antibiotic and incubated at 37 °C (220 rpm) until an OD_{600} of around 0.4–0.7 was reached. 10 mL of melted LB soft (0.75%) agar were inoculated with the day cultures to achieve a final OD_{600} of 0.01 and poured onto the surface of the LB plates. The fungal strain *P. chrysogenum* was kept as a spore suspension at –20 ˚C and used in inoculation of LB soft (0.75%) agar (100 μL in 10 mL LB soft agar). After a drying period of at least 10 min, the microorganism lawn was inoculated with 15 μL of the bilothiazodes (**5**,**6** [5.8 mg/mL]; **7** [6.1 mg/mL]; **8** [7.9 mg/mL]; **9** [7.1 mg/mL] and **10** [7.9 mg/mL]). 15 μL of either an antibiotic (positive control; nisin (40 mg/mL) for *B. subtilis* W168 and *B. subtilis* subsp. *spizizenii* ATCC 6633, ciprofloxacin (200 μg/mL) for all pathogenic bacterial strains, norfloxacin (100 μg/mL) for *E. coli* K12, amphotericin B (250 μg/mL) for *P. chrysogenum*) and a 99.8% (v/v) DMSO solution (negative control) were applied to the surface of the plates after spread coating. Subsequently, another drying period was conducted to allow the pure compounds to be completely absorbed into the agar. Afterward, all plates were incubated upside down overnight at 37 °C for bacterial strains and 28

°C for *P. chrysogenum*. Plates were documented photographically on a black background using a P.CAM360 (1.48x magnification, overhead light level 3).

Determination of inhibitory concentrations

The sensitivity of *B. subtilis* W168, *S. aureus* ATCC 25923 and *E. coli* K-12 towards bilothiazoles were determined in LB medium. Fresh cultures were grown to an optical density (OD_{600}) of about 0.5 (mid-log) and then diluted to a final OD_{600} of 0.05. Subsequently, 95 µL of the diluted day culture were added to each well and grown in Synergy™ HTX multi-mode microplate reader from BioTek (Winooski, USA) at 37 °C with aeration. After one hour of incubation, serial dilutions (1:2) of the bilothiazodes were prepared and 5 µL of each concentration were added to each well. DMSO (5%, v/v) was used as the negative control. For the determination of inhibitory concentrations of bilothiazoles, the OD_{600} was measured in 5 min intervals for at least 12 h. Microplate reader experiments were performed in biological and technical triplicates.

Luciferase-Assays in LB-liquid medium

The potential molecular functions of the bilothiazoles were determinated using the *B. subtilis* biosensor strains (TMB1617, TMB1619, TMB2120, TMB5611, TMB5830, TMB5831, TMB5845 and TMB5600) harbouring pBS3C*lux*-derivates. Therefore, overnight cultures were grown in LB supplemented with chloramphenicol (final concentration 5 µg/ml) for selection. Day cultures, without antibiotics, were inoculated 1:250 in fresh LB-medium and grown to an OD_{600} of 0.3–0.4. Subsequently, cells were diluted to an OD_{600} 0.05 and 95 µl were incubated in a 96-microtiter well plate (black walls, clear bottom, Greiner Bio-One, Frickenhausen, Germany) at 37 °C using a Synergy™ HTX plate reader (BioTek® Intruments GmbH, Bad Friedrichshall, Germany). Luminescence and OD_{600} were measured in 5 min intervals. After one hour, the biosensor cells were induced with 5 µl of bilothiazoles and antibiotics as a positive control (bacitracin for TMB1617 and TMB1619, nisin for TMB2120, penicillin G for TMB5611, norfloxacin for TMB5830, erythromycin for TMB5831, rifampicin for TMB5845 and amphotericin B for TMB5600), to get final concentrations of 0.3 µg/ml norfloxacin, 0.01 µg/ml penicillin G, 152.5 µg/ml bilothiazole C (**7**), 83.75 µg/ml bilothiazole E (**9**) and 87.5 µg/ml bilothiazole F (**10**). The microplate was subsequently placed back in the microplate reader to continue luminescence and OD_{600} measurements in the aforementioned intervals for 11 h. Quantification of luminescence was achieved by calculating relative luminescence units (RLU), or the luminescence divided by the OD_{600} at a given time point. Visualization

of biosensor induction was realized by plotting RLU as a function of time using GraphPad Prism (version 5, San Diego, California). Experiments were performed in biological and technical triplicates.

Analytical Data

Bilothiazole A (**5**):

^{1}H-NMR (600 MHz, DMSO-d_6) δ = 8.31 (s, 1H), 7.56 (dd, *J* = 8.0, 1.5 Hz, 1H), 6.93−6.91 (m, 1H), 6.81 (dd, *J* = 15.6, 7.8 Hz, 1H), 5.31 (dd, *J* = 9.6, 8.2 Hz, 1H), 3.62 (ddd, *J* = 19.3, 11.1, 8.9 Hz, 2H) ppm. ^{13}C-NMR (151 MHz, DMSO-d6) δ = 171.9, 163.8, 163.5, 146.6, 146.0, 144.2, 127.1, 121.9, 119.5, 117.5, 116.6, 78.4, 34.4 Hz. HRMS (ESI+): m/z = 323.0155 $[M+H]^+$, calc.: 323.0155.

Bilothiazole B (**6**):

^{1}H-NMR (600 MHz, DMSO-d_6) δ = 8.62 (d, *J* = 8.1 Hz, 1H), 8.30 (s, 1H), 7.76−7.74 (m, 1H), 6.93−6.91 (m, 1H), 6.81 (dd, *J* = 15.6, 7.8 Hz, 1H), 4.45 (td, *J* = 7.6, 4.6 Hz, 1H), 3.10−3.00 (m, 2H) ppm. ^{13}C-NMR (151 MHz, DMSO-d6) δ = 171.6, 163.7, 160.6, 148.0, 146.1, 144.3, 127.1, 124.6, 119.6, 117.9, 116.7, 54.3, 25.4 Hz. HRMS (ESI+): m/z = 341.0263 $[M+H]^+$, calc.: 341.0260.

Bilothiazole C (**7**):

^{1}H-NMR (600 MHz, DMSO-d_6) δ = 11.26 (bs, 1H), 8.32 (s, 1H), 8.14 (dd, *J* = 7.9, 1.7 Hz, 1H), 7.34 (ddd, *J* = 8.4, 7.3, 1.7 Hz, 1H), 7.05 (dd, *J* = 8.2, 0.8 Hz, 1H), 6.99 (ddd, *J* = 7.9, 7.2, 1.1 Hz, 1H), 5.30 (dd, *J* = 9.6, 8.2 Hz, 1H), 3.67 (dd, *J* = 11.1, 9.8 Hz, 1H), 3.57 (dd, *J* = 11.1, 8.2 Hz, 1H) ppm. ^{13}C-NMR (151 MHz, DMSO-d6) δ = 171.9, 163.8, 162.9, 155.1, 146.8, 131.5, 127.4, 122.1, 119.7, 118.8, 116.5, 78.45, 34.37 ppm. HRMS (ESI+): m/z = 307.0206 $[M+H]^+$, calc.: 307.0206. $[\alpha]_D^{20}$ = +34.5 (*c* 2.3, MeOH). The spectroscopic data was in agreement to those reported in the literature. (*45*)

Bilothiazole D (**8**):

^{1}H-NMR (600 MHz, Methanol-d_4) δ = 8.24 (s, 1H), 8.20 (dd, *J* = 7.9, 1.6 Hz, 1H), 7.33 (ddd, *J* = 8.3, 7.3, 1.7 Hz, 1H), 7.01 (m, 1H), 6.98 (dd, *J* = 8.0, 0.9 Hz, 1H), 4.86 (dd, *J* = 5.8, 4.7 Hz, 1H), 3.15 (qd, *J* = 14.6, 5.3 Hz, 2H) ppm. ^{13}C-NMR (151 MHz, Methanol-d4) δ = 173.0, 166.8, 163.3, 156.9, 149.2, 132.8, 129.1, 125.2, 120.9, 120.0, 117.5, 55.70, 26.82 ppm. HRMS (ESI+): m/z = 325.0324 $[M+H]^+$, calc.: 325.0311.

Bilothiazole E (**9**):

^{1}H-NMR (600 MHz, DMSO-d_6) δ = 11.15 (bs, 1H), 8.27 (s, 1H), 8.01 (d, *J* = 8.0 Hz, 1H), 6.85 (s, 1H), 6.81 (dd, *J* = 8.2, 2.1 Hz, 1H), 5.29 (dd, *J* = 9.7, 8.2 Hz, 1H), 3.66 (dd, *J* = 11.1, 9.7 Hz, 1H), 3.57 (dd, *J*

= 11.2, 8.2 Hz, 1H), 2.29 (s, 3H) ppm. ^{13}C-NMR (151 MHz, DMSO-d6) δ = 171.9, 163.8, 163.3, 155.1, 146.7, 141.7, 127.3, 121.5, 120.7, 116.8, 116.3, 78.45, 34.36, 21.12 ppm. HRMS (ESI+): m/z = 321.0360 $[M+H]^+$, calc.: 321.0362. $[\alpha]_D^{20}$ = +27.0 (*c* 7.8, MeOH).

Bilothiazole F (**10**):

^{1}H-NMR (600 MHz, DMSO-d_6) δ = 11.27 (bs, 1H), 8.52 (s, 1H), 8.26–8.24 (m, 1H), 7.58–7.55 (m, 1H), 7.49 (dd, *J* = 8.5, 4.5 Hz, 1H), 5.36 (dd, *J* = 9.6, 8.2 Hz, 1H), 3.70 (ddd, *J* = 19.3, 11.2, 9.0 Hz, 2H) ppm. ^{13}C-NMR (151 MHz, DMSO-d6) δ = 171.6, 169.5, 162.2, 152.2, 147.1, 141.5, 134.1, 127.2, 125.4, 123.8, 78.43, 34.85 ppm. HRMS (ESI+): m/z = 308.0158 $[M+H]^+$, calc.: 308.0158. $[\alpha]_D^{20}$ = +4.1 (*c* 4.9, MeOH).

Data Availability

All data generated during this study are deposited in the supplementary information and are additionally available from the corresponding author on request. ^{1}H and ^{13}C-NMR spectra for compounds **5**–**10** can be found in the supplementary information (Figures S22–49).

Author Contributions

M.H. and T.A.M.G. designed the research project. M.H. conducted all work associated with BGC cloning, compound expression and isolation and chemical analytics. D.I., W.J, K.P.J. and T.M. planned and conducted all work on the in-depth characterization of the bioactivities of the bilothiazoles. M.L. and G.Z. performed bioinformatic analyses. G.Z., T.M., K.P.J., and T.A.M.G. provided materials and infrastructure and secured funding for the project. M.H. and T.A.M.G. wrote the manuscript, which all authors reviewed and revised.

Acknowledgements

We thank Dr. T. Lübken and his team (TU Dresden, Organic Chemistry I) for recording NMR spectra. This work was funded by the Deutsche Forschungsgemeinschaft (DFG, German Research Foundation, project ID 395357507—SFB 1371, Microbiome Signatures to G.Z., K.P.J. and T.A.M.G.).

References

1. Qin, J.; Li, R.; Raes, J.; Arumugam, M.; Burgdorf, K. S.; Manichanh, C.; Nielsen, T.; Pons, N.; Levenez, F.; Yamada, T.; Mende, D. R.; Li, J.; Xu, J.; Li, S.; Li, D.; Cao, J.; Wang, B.; Liang, H.; Zheng, H.; Xie, Y.; Tap, J.; Lepage, P.; Bertalan, M.; Batto, J.-M.; Hansen, T.; Le Paslier, D.;

Linneberg, A.; Nielsen, H. B.; Pelletier, E.; Renault, P.; Sicheritz-Ponten, T.; Turner, K.; Zhu, H.; Yu, C.; Li, S.; Jian, M.; Zhou, Y.; Li, Y.; Zhang, X.; Li, S.; Qin, N.; Yang, H.; Wang, J.; Brunak, S.; Doré, J.; Guarner, F.; Kristiansen, K.; Pedersen, O.; Parkhill, J.; Weissenbach, J.; Bork, P.; Ehrlich, S. D.; Wang, J. A human gut microbial gene catalogue established by metagenomic sequencing. *Nature* **2010,** *464* (7285), 59–65. DOI: 10.1038/nature08821.

2. Frank, D. N.; St Amand, A. L.; Feldman, R. A.; Boedeker, E. C.; Harpaz, N.; Pace, N. R. Molecular-phylogenetic characterization of microbial community imbalances in human inflammatory bowel diseases. *Proc. Natl. Acad. Sci. U. S. A.* **2007,** *104* (34), 13780–13785. DOI: 10.1073/pnas.0706625104.

3. Jandhyala, S. M.; Talukdar, R.; Subramanyam, C.; Vuyyuru, H.; Sasikala, M.; Nageshwar Reddy, D. Role of the normal gut microbiota. *World J. Gastroenterol.* **2015,** *21* (29), 8787–8803. DOI: 10.3748/wjg.v21.i29.8787.

4. Rinninella, E.; Raoul, P.; Cintoni, M.; Franceschi, F.; Miggiano, G. A. D.; Gasbarrini, A.; Mele, M. C. What is the Healthy Gut Microbiota Composition? A Changing Ecosystem across Age, Environment, Diet, and Diseases. *Microorganisms* **2019,** *7* (1). DOI: 10.3390/microorganisms7010014.

5. Sekirov, I.; Russell, S. L.; Antunes, L. C. M.; Finlay, B. B. Gut microbiota in health and disease. *Physiol. Rev.* **2010,** *90* (3), 859–904. DOI: 10.1152/physrev.00045.2009.

6. Schneditz, G.; Rentner, J.; Roier, S.; Pletz, J.; Herzog, K. A. T.; Bücker, R.; Troeger, H.; Schild, S.; Weber, H.; Breinbauer, R.; Gorkiewicz, G.; Högenauer, C.; Zechner, E. L. Enterotoxicity of a nonribosomal peptide causes antibiotic-associated colitis. *Proc. Natl. Acad. Sci. U. S. A.* **2014,** *111* (36), 13181–13186. DOI: 10.1073/pnas.1403274111.

7. Gubatan, J.; Holman, D. R.; Puntasecca, C. J.; Polevoi, D.; Rubin, S. J. S.; Rogalla, S. Antimicrobial peptides and the gut microbiome in inflammatory bowel disease. *World J. Gastroenterol.* **2021,** *27* (43), 7402–7422. DOI: 10.3748/wjg.v27.i43.7402.

8. Zong, X.; Fu, J.; Xu, B.; Wang, Y.; Jin, M. Interplay between gut microbiota and antimicrobial peptides. *Anim. Nutr.* **2020,** *6* (4), 389–396. DOI: 10.1016/j.aninu.2020.09.002.

9. Saleem, M.; Nazir, M.; Ali, M. S.; Hussain, H.; Lee, Y. S.; Riaz, N.; Jabbar, A. Antimicrobial natural products: an update on future antibiotic drug candidates. *Nat. Prod. Rep.* **2010,** *27* (2), 238–254. DOI: 10.1039/B916096E.

10. Davies, J. What are antibiotics? Archaic functions for modern activities. *Mol. Microbiol.* **1990,** *4* (8), 1227–1232. DOI: 10.1111/j.1365-2958.1990.tb00701.x.
11. Garcia-Gutierrez, E.; Mayer, M. J.; Cotter, P. D.; Narbad, A. Gut microbiota as a source of novel antimicrobials. *Gut Microbes* **2019,** *10* (1), 1–21. DOI: 10.1080/19490976.2018.1455790.
12. Proal, A. D.; Lindseth, I. A.; Marshall, T. G. Microbe-Microbe and Host-Microbe Interactions Drive Microbiome Dysbiosis and Inflammatory Processes. *Discovery Medicine* **2017,** *23* (124), 51–60.
13. Wang, L.; Ravichandran, V.; Yin, Y.; Yin, J.; Zhang, Y. Natural Products from Mammalian Gut Microbiota. *Trends Biotechnol.* **2019,** *37* (5), 492–504. DOI: 10.1016/j.tibtech.2018.10.003.
14. King, A. M.; Zhang, Z.; Glassey, E.; Siuti, P.; Clardy, J.; Voigt, C. A. Systematic mining of the human microbiome identifies antimicrobial peptides with diverse activity spectra. *Nat. Microbiol.* **2023. DOI:** 10.1038/s41564-023-01524-6.
15. Donia, M. S.; Cimermancic, P.; Schulze, C. J.; Wieland Brown, L. C.; Martin, J.; Mitreva, M.; Clardy, J.; Linington, R. G.; Fischbach, M. A. A systematic analysis of biosynthetic gene clusters in the human microbiome reveals a common family of antibiotics. *Cell* **2014,** *158* (6), 1402–1414. DOI: 10.1016/j.cell.2014.08.032.
16. Hirsch, P.; Tagirdzhanov, A.; Kushnareva, A.; Olkhovskii, I.; Graf, S.; Schmartz, G. P.; Hegemann, J. D.; Bozhüyük, K. A. J.; Müller, R.; Keller, A.; Gurevich, A. ABC-HuMi: the Atlas of Biosynthetic Gene Clusters in the Human Microbiome. *Nucleic. Acids. Res.* **2024,** *52* (D1), D579-D585. DOI: 10.1093/nar/gkad1086.
17. Lawlor, M. S.; O'connor, C.; Miller, V. L. Yersiniabactin is a virulence factor for Klebsiella pneumoniae during pulmonary infection. *Infect. Immun.* **2007,** *75* (3), 1463–1472. DOI: 10.1128/IAI.00372-06.
18. Cox, C. D.; Rinehart, K. L.; Moore, M. L.; Cook, J. C. Pyochelin: novel structure of an iron-chelating growth promoter for Pseudomonas aeruginosa. *Proc. Natl. Acad. Sci. U. S. A.* **1981,** *78* (7), 4256–4260. DOI: 10.1073/pnas.78.7.4256.
19. Raymond, K. N.; Dertz, E. A.; Kim, S. S. Enterobactin: an archetype for microbial iron transport. *Proc. Natl. Acad. Sci. U. S. A.* **2003,** *100* (7), 3584–3588. DOI: 10.1073/pnas.0630018100.
20. Blin, K.; Shaw, S.; Kloosterman, A. M.; Charlop-Powers, Z.; van Wezel, G. P.; Medema, M. H.; Weber, T. antiSMASH 6.0: improving cluster detection and comparison capabilities. *Nucleic. Acids. Res.* **2021,** *49* (W1), W29-W35. DOI: 10.1093/nar/gkab335.

21. Büttner, H.; Hörl, J.; Krabbe, J.; Hertweck, C. Discovery and Biosynthesis of Anthrochelin, a Growth-Promoting Metallophore of the Human Pathogen Luteibacter anthropi. *ChemBioChem* **2023,** *24* (17), e202300322. DOI: 10.1002/cbic.202300322.
22. Gao, Y.; Walt, C.; Bader, C. D.; Müller, R. Genome-Guided Discovery of the Myxobacterial Thiolactone-Containing Sorangibactins. *ACS Chem. Biol.* **2023,** *18* (4), 924–932. DOI: 10.1021/acschembio.3c00063.
23. Ellermann, M.; Gharaibeh, R. Z.; Fulbright, L.; Dogan, B.; Moore, L. N.; Broberg, C. A.; Lopez, L. R.; Rothemich, A. M.; Herzog, J. W.; Rogala, A.; Gordon, I. O.; Rieder, F.; Brouwer, C. R.; Simpson, K. W.; Jobin, C.; Sartor, R. B.; Arthur, J. C. Yersiniabactin-Producing Adherent/Invasive Escherichia coli Promotes Inflammation-Associated Fibrosis in Gnotobiotic Il10-/- Mice. *Infect. Immun.* **2019,** *87* (11). DOI: 10.1128/IAI.00587-19.
24. Hohmann, M.; Brunner, V.; Johannes, W.; Schum, D.; Carroll, L. M.; Liu, T.; Sasaki, D.; Bosch, J.; Clavel, T.; Sieber, S. A.; Zeller, G.; Tschurtschenthaler, M.; Janßen, K.-P.; Gulder, T. A. M. Bacillamide D produced by Bacillus cereus from the mouse intestinal bacterial collection (miBC) is a potent cytotoxin in vitro. *Commun. Biol.* **2024,** *7* (1), 655. DOI: 10.1038/s42003-024-06208-3.
25. Almeida, A.; Nayfach, S.; Boland, M.; Strozzi, F.; Beracochea, M.; Shi, Z. J.; Pollard, K. S.; Sakharova, E.; Parks, D. H.; Hugenholtz, P.; Segata, N.; Kyrpides, N. C.; Finn, R. D. A unified catalog of 204,938 reference genomes from the human gut microbiome. *Nat. Biotechnol.* **2021,** *39* (1), 105–114. DOI: 10.1038/s41587-020-0603-3.
26. Mende, D. R.; Letunic, I.; Maistrenko, O. M.; Schmidt, T. S. B.; Milanese, A.; Paoli, L.; Hernández-Plaza, A.; Orakov, A. N.; Forslund, S. K.; Sunagawa, S.; Zeller, G.; Huerta-Cepas, J.; Coelho, L. P.; Bork, P. proGenomes2: an improved database for accurate and consistent habitat, taxonomic and functional annotations of prokaryotic genomes. *Nucleic. Acids. Res.* **2020,** *48* (D1), D621-D625. DOI: 10.1093/nar/gkz1002.
27. Steinegger, M.; Söding, J. MMseqs2 enables sensitive protein sequence searching for the analysis of massive data sets. *Nat. Biotechnol.* **2017,** *35* (11), 1026–1028. DOI: 10.1038/nbt.3988.
28. Baron, E. J.; Summanen, P.; Downes, J.; Roberts, M. C.; Wexler, H.; Finegold, S. M. Bilophila wadsworthia, gen. nov. and sp. nov., a unique gram-negative anaerobic rod recovered from appendicitis specimens and human faeces. *J. Gen. Microbiol.* **1989,** *135* (12), 3405–3411. DOI: 10.1099/00221287-135-12-3405.

29. Baron, E. J. Bilophila wadsworthia: a unique Gram-negative anaerobic rod. *Anaerobe* **1997,** *3* (2-3), 83–86. DOI: 10.1006/anae.1997.0075.
30. Peck, S. C.; Denger, K.; Burrichter, A.; Irwin, S. M.; Balskus, E. P.; Schleheck, D. A glycyl radical enzyme enables hydrogen sulfide production by the human intestinal bacterium Bilophila wadsworthia. *Proc. Natl. Acad. Sci. U. S. A.* **2019,** *116* (8), 3171–3176. DOI: 10.1073/pnas.1815661116.
31. Edgar, R. C. Muscle5: High-accuracy alignment ensembles enable unbiased assessments of sequence homology and phylogeny. *Nat. Commun.* **2022,** *13* (1), 6968. DOI: 10.1038/s41467-022-34630-w.
32. Price, M. N.; Dehal, P. S.; Arkin, A. P. FastTree 2--approximately maximum-likelihood trees for large alignments. *PLoS One* **2010,** *5* (3), e9490. DOI: 10.1371/journal.pone.0009490.
33. Huerta-Cepas, J.; Serra, F.; Bork, P. ETE 3: Reconstruction, Analysis, and Visualization of Phylogenomic Data. *Mol. Biol. Evol.* **2016,** *33* (6), 1635–1638. DOI: 10.1093/molbev/msw046.
34. Zulkower, V.; Rosser, S. DNA Features Viewer: a sequence annotation formatting and plotting library for Python. *Bioinformatics* **2020,** *36* (15), 4350–4352. DOI: 10.1093/bioinformatics/btaa213.
35. Schoch, C. L.; Ciufo, S.; Domrachev, M.; Hotton, C. L.; Kannan, S.; Khovanskaya, R.; Leipe, D.; Mcveigh, R.; O'Neill, K.; Robbertse, B.; Sharma, S.; Soussov, V.; Sullivan, J. P.; Sun, L.; Turner, S.; Karsch-Mizrachi, I. NCBI Taxonomy: a comprehensive update on curation, resources and tools. *Database* **2020,** *2020. DOI:* 10.1093/database/baaa062.
36. Ruscheweyh, H.-J.; Milanese, A.; Paoli, L.; Karcher, N.; Clayssen, Q.; Keller, M. I.; Wirbel, J.; Bork, P.; Mende, D. R.; Zeller, G.; Sunagawa, S. Cultivation-independent genomes greatly expand taxonomic-profiling capabilities of mOTUs across various environments. *Microbiome* **2022,** *10* (1), 212. DOI: 10.1186/s40168-022-01410-z.
37. Skinnider, M. A.; Merwin, N. J.; Johnston, C. W.; Magarvey, N. A. PRISM 3: expanded prediction of natural product chemical structures from microbial genomes. *Nucleic. Acids. Res.* **2017,** *45* (W1), W49-W54. DOI: 10.1093/nar/gkx320.
38. Greunke, C.; Duell, E. R.; D'Agostino, P. M.; Glöckle, A.; Lamm, K.; Gulder, T. A. M. Direct Pathway Cloning (DiPaC) to unlock natural product biosynthetic potential. *Metab. Eng.* **2018,** *47*, 334–345. DOI: 10.1016/j.ymben.2018.03.010.

39. D'Agostino, P. M.; Gulder, T. A. M. Direct Pathway Cloning Combined with Sequence- and Ligation-Independent Cloning for Fast Biosynthetic Gene Cluster Refactoring and Heterologous Expression. *ACS Synth. Biol.* **2018,** *7* (7), 1702–1708. DOI: 10.1021/acssynbio.8b00151.

40. Duell, E. R.; D'Agostino, P. M.; Shapiro, N.; Woyke, T.; Fuchs, T. M.; Gulder, T. A. M. Direct pathway cloning of the sodorifen biosynthetic gene cluster and recombinant generation of its product in E. coli. *Microb. Cell Fact.* **2019,** *18* (1), 32. DOI: 10.1186/s12934-019-1080-6.

41. Eusébio, N.; Castelo-Branco, R.; Sousa, D.; Preto, M.; D'Agostino, P.; Gulder, T. A. M.; Leão, P. N. Discovery and Heterologous Expression of Microginins from Microcystis aeruginosa LEGE 91341. *ACS Synth. Biol.* **2022,** *11* (10), 3493–3503. DOI: 10.1021/acssynbio.2c00389.

42. Ouyang, X.; D'Agostino, P. M.; Wahlsten, M.; Delbaje, E.; Jokela, J.; Permi, P.; Gaiani, G.; Poso, A.; Bartos, P.; Gulder, T. A. M.; Koistinen, H.; Fewer, D. P. Direct pathway cloning and expression of the radiosumin biosynthetic gene cluster. *Org. Biomol. Chem.* **2023,** *21* (23), 4893–4908. DOI: 10.1039/d3ob00385j.

43. Pfeifer, B. A.; Admiraal, S. J.; Gramajo, H.; Cane, D. E.; Khosla, C. Biosynthesis of complex polyketides in a metabolically engineered strain of E. coli. *Science* **2001,** *291* (5509), 1790–1792. DOI: 10.1126/science.1058092.

44. Jeong, J.-Y.; Yim, H.-S.; Ryu, J.-Y.; Lee, H. S.; Lee, J.-H.; Seen, D.-S.; Kang, S. G. One-step sequence- and ligation-independent cloning as a rapid and versatile cloning method for functional genomics studies. *Appl. Environ. Microbiol.* **2012,** *78* (15), 5440–5443. DOI: 10.1128/AEM.00844-12.

45. Mislin, G. L.; Burger, A.; Abdallah, M. A. Synthesis of new thiazole analogues of pyochelin, a siderophore of Pseudomonas aeruginosa and Burkholderia cepacia. A new conversion of thiazolines into thiazoles. *Tetrahedron* **2004,** *60* (52), 12139–12145. DOI: 10.1016/j.tet.2004.10.030.

46. Quadri, L. E.; Keating, T. A.; Patel, H. M.; Walsh, C. T. Assembly of the Pseudomonas aeruginosa nonribosomal peptide siderophore pyochelin: In vitro reconstitution of aryl-4, 2-bisthiazoline synthetase activity from PchD, PchE, and PchF. *Biochemistry* **1999,** *38* (45), 14941–14954. DOI: 10.1021/bi991787c.

47. Reimmann, C.; Patel, H. M.; Serino, L.; Barone, M.; Walsh, C. T.; Haas, D. Essential PchG-dependent reduction in pyochelin biosynthesis of Pseudomonas aeruginosa. *J. Bacteriol.* **2001,** *183* (3), 813–820. DOI: 10.1128/JB.183.3.813–820.2001.

48. Ohlemacher, S. I.; Giblin, D. E.; d'Avignon, D. A.; Stapleton, A. E.; Trautner, B. W.; Henderson, J. P. Enterobacteria secrete an inhibitor of Pseudomonas virulence during clinical bacteriuria. *J. Clin. Invest.* **2017,** *127* (11), 4018–4030. DOI: 10.1172/JCI92464.

49. Young, I. G.; Langman, L.; Luke, R. K.; Gibson, F. Biosynthesis of the iron-transport compound enterochelin: mutants of Escherichia coli unable to synthesize 2,3-dihydroxybenzoate. *J. Bacteriol.* **1971,** *106* (1), 51–57. DOI: 10.1128/jb.106.1.51-57.1971.

50. Hancock, R. E.; Hantke, K.; Braun, V. Iron transport in Escherichia coli K-12. 2,3-Dihydroxybenzoate-promoted iron uptake. *Arch. Microbiol.* **1977,** *114* (3), 231–239. DOI: 10.1007/BF00446867.

51. Wilson, M. R.; Jiang, Y.; Villalta, P. W.; Stornetta, A.; Boudreau, P. D.; Carrá, A.; Brennan, C. A.; Chun, E.; Ngo, L.; Samson, L. D.; Engelward, B. P.; Garrett, W. S.; Balbo, S.; Balskus, E. P. The human gut bacterial genotoxin colibactin alkylates DNA. *Science* **2019,** *363* (6428). DOI: 10.1126/science.aar7785.

52. Xue, M.; Kim, C. S.; Healy, A. R.; Wernke, K. M.; Wang, Z.; Frischling, M. C.; Shine, E. E.; Wang, W.; Herzon, S. B.; Crawford, J. M. Structure elucidation of colibactin and its DNA cross-links. *Science* **2019,** *365* (6457). DOI: 10.1126/science.aax2685.

53. Cox, M. M. Regulation of bacterial RecA protein function. *Crit. Rev. Biochem. Mol. Biol.* **2007,** *42* (1), 41–63. DOI: 10.1080/10409230701260258.

54. Milzarek, T. M.; Stevanovic, M.; Milivojevic, D.; Vojnovic, S.; Iliasov, D.; Wolf, D.; Mascher, T.; Nikodinovic-Runic, J.; Gulder, T. A. M. Antibiotic Potential of the Ambigol Cyanobacterial Natural Product Class and Simplified Synthetic Analogs. *ACS Infect. Dis.* **2023,** *9* (10), 1941–1948. DOI: 10.1021/acsinfecdis.3c00232.

55. Hussain, M.; Pastor, F. I.; Lampen, J. O. Cloning and sequencing of the blaZ gene encoding beta-lactamase III, a lipoprotein of Bacillus cereus 569/H. *J. Bacteriol.* **1987,** *169* (2), 579–586. DOI: 10.1128/jb.169.2.579-586.1987.

56. Olsen, J. E.; Christensen, H.; Aarestrup, F. M. Diversity and evolution of blaZ from Staphylococcus aureus and coagulase-negative staphylococci. *J. Antimicrob. Chemother.* **2006,** *57* (3), 450–460. DOI: 10.1093/jac/dki492.

57. Kallifidas, D.; Pascoe, B.; Owen, G. A.; Strain-Damerell, C. M.; Hong, H.-J.; Paget, M. S. B. The zinc-responsive regulator Zur controls expression of the coelibactin gene cluster in Streptomyces coelicolor. *J. Bacteriol.* **2010,** *192* (2), 608–611. DOI: 10.1128/jb.01022-09.

58. Carroll, L. M.; Larralde, M.; Fleck, J. S.; Ponnudurai, R.; Milanese, A.; Cappio, E.; Zeller, G. Accurate de novo identification of biosynthetic gene clusters with GECCO. *bioRxiv* **2021. DOI:** 10.1101/2021.05.03.442509.
59. Camacho, C.; Coulouris, G.; Avagyan, V.; Ma, N.; Papadopoulos, J.; Bealer, K.; Madden, T. L. BLAST+: architecture and applications. *BMC Bioinformatics* **2009,** *10*, 421. DOI: 10.1186/1471-2105-10-421.
60. Steinegger, M.; Söding, J. Clustering huge protein sequence sets in linear time. *Nat. Commun.* **2018,** *9* (1), 2542. DOI: 10.1038/s41467-018-04964-5.
61. Kearse, M.; Moir, R.; Wilson, A.; Stones-Havas, S.; Cheung, M.; Sturrock, S.; Buxton, S.; Cooper, A.; Markowitz, S.; Duran, C.; Thierer, T.; Ashton, B.; Meintjes, P.; Drummond, A. Geneious Basic: an integrated and extendable desktop software platform for the organization and analysis of sequence data. *Bioinformatics* **2012,** *28* (12), 1647–1649. DOI: 10.1093/bioinformatics/bts199.
62. van den Belt, M.; Gilchrist, C.; Booth, T. J.; Chooi, Y.-H.; Medema, M. H.; Alanjary, M. CAGECAT: The CompArative GEne Cluster Analysis Toolbox for rapid search and visualisation of homologous gene clusters. *BMC Bioinformatics* **2023,** *24* (1), 181. DOI: 10.1186/s12859-023-05311-2.
63. D'Agostino, P. M.; Seel, C. J.; Ji, X.; Gulder, T.; Gulder, T. A. M. Biosynthesis of cyanobacterin, a paradigm for furanolide core structure assembly. *Nat. Chem. Biol.* **2022,** *18* (6), 652–658. DOI: 10.1038/s41589-022-01013-7.